AUGUST 12 2024

Asymmetric triangular body-cover model of the vocal folds with bilateral intrinsic muscle activation

Jesús A. Parra ; Carlos Calvache ; Gabriel A. Alzamendi ; Emiro J. Ibarra ; Leonardo Soláque ; Sean D. Peterson ; Matías Zañartu

J. Acoust. Soc. Am. 156, 939–953 (2024)
https://doi.org/10.1121/10.0028164

JASA ARTICLE

Asymmetric triangular body-cover model of the vocal folds with bilateral intrinsic muscle activation

Jesús A. Parra,[1,a] Carlos Calvache,[2,3] Gabriel A. Alzamendi,[4,5] Emiro J. Ibarra,[1] Leonardo Soláque,[2] Sean D. Peterson,[6] and Matías Zañartu[1]

[1]*Department of Electronic Engineering, Universidad Técnica Federico Santa Maria, Valparaíso, Chile*

[2]*Department of Mechatronics Engineering, Universidad Militar, Bogota, Colombia*

[3]*Department Communication Sciences and Disorders, Corporación Universitaria Iberoamericana, Bogotá, Colombia*

[4]*Institute for Research and Development on Bioengineering and Bioinformatics, Consejo Nacional de Investigaciones Científicas y Técnicas, Universidad Nacional de Entre Ríos, Oro Verde, Entre Ríos, Argentina*

[5]*Facultad de Ingeniería, Universidad Nacional de Entre Ríos, Entre Ríos, Argentina*

[6]*Department of Mechanical and Mechatronics Engineering, University of Waterloo, Waterloo, Ontario, Canada*

ABSTRACT:

Many voice disorders are linked to imbalanced muscle activity and known to exhibit asymmetric vocal fold vibration. However, the relation between imbalanced muscle activation and asymmetric vocal fold vibration is not well understood. This study introduces an asymmetric triangular body-cover model of the vocal folds, controlled by the activation of bilateral intrinsic laryngeal muscles, to investigate the effects of muscle imbalance on vocal fold oscillation. Various scenarios were considered, encompassing imbalance in individual muscles and muscle pairs, as well as accounting for asymmetry in lumped element parameters. Measurements of amplitude and phase asymmetries were employed to match the oscillatory behavior of two pathological cases: unilateral paralysis and muscle tension dysphonia. The resulting simulations exhibit muscle imbalance consistent with expectations in the composition of these voice disorders, yielding asymmetries exceeding 30% for paralysis and below 5% for dysphonia. This underscores the relevance of muscle imbalance in representing phonatory scenarios and its potential for characterizing asymmetry in vocal fold vibration. © *2024 Acoustical Society of America*. https://doi.org/10.1121/10.0028164

(Received 18 January 2024; revised 9 July 2024; accepted 12 July 2024; published online 12 August 2024)

[Editor: Zhaoyan Zhang] Pages: 939–953

I. INTRODUCTION

The production of human voice sounds results from intricate physical interactions within the speech organs, governed by a sophisticated neuromuscular control system (Story, 2015). Vocal physiology can be elucidated through (1) the nearly stable subglottal driving pressure, (2) the intricate interplay of acoustic pressure, flow, and vocal fold (VF) tissue at the glottal level, and (3) the propagation and modulation of voice sound throughout the supraglottal vocal tract (Story, 2002; Zhang, 2016b). A plethora of numerical models exist, varying in physiological fidelity, mathematical intricacy, and computational demands (Calvache *et al.*, 2023; Döllinger *et al.*, 2023). Among these, lumped-element models based on non-linear mechanical components, like coupled mass-spring-damper systems, hold particular utility for comprehensive investigations of underlying glottal phenomena (Erath *et al.*, 2013). These models include biomechanical characteristics of VF tissues (Titze and Story, 2002), transversal mucosal wave (Perrine and Scherer, 2023; Story, 2002), aeroacoustic interactions (Horáček *et al.*, 2007; Zañartu *et al.*, 2007), glottal geometry (Galindo *et al.*, 2017), and laryngeal muscle control (Ji *et al.*, 2022; Titze and Hunter, 2007). A notable characteristic of lumped-element models is that achieve a suitable balance between computation burden and physiological significance.

While numerical models have traditionally been employed to simulate physiological mechanisms in modal and typical phonation, ongoing refinements have expanded their applicability to variables describing vocal function in pathological contexts. Modeling of vocal function provides a framework for exploring biomechanical aspects of impaired phonation, including the identification of biomechanical properties (Jiang *et al.*, 2006; Palaparthi *et al.*, 2019; Samlan and Story, 2017; Tao and Jiang, 2007; Vampola *et al.*, 2016), VF geometrical properties (Geng *et al.*, 2020; Li *et al.*, 2020; McCollum *et al.*, 2023; Zhang, 2021, 2023), variations in intrinsic muscular control of the larynx (Chhetri *et al.*, 2009; Manríquez *et al.*, 2019; Movahhedi *et al.*, 2021), and changes in the aeromechanical-acoustic interaction (Chen *et al.*, 2020; Erath *et al.*, 2019; Yokota *et al.*, 2019; Zhang, 2016a, 2018).

VF asymmetry holds significant relevance for clinical voice research, potentially playing a pivotal role for studying the onset of dysphonias and other vocal disorders

[a]Email: jeaparrape@gmail.com

(Pickup and Thomson, 2009). Prior studies employing modeling techniques have investigated asymmetries in VF to comprehend their underlying etiology and explore potential clinical interventions (Lucero *et al.*, 2020; Mehta *et al.*, 2011; Zhang and Luu, 2012). However, within the context of lumped-element models, asymmetry has primarily focused on geometrical and mechanical distinctions between the folds (Dresel *et al.*, 2006; Erath *et al.*, 2011; Mehta *et al.*, 2011; Sommer *et al.*, 2013; Steinecke and Herzel, 1995; Xue *et al.*, 2010).

Motivated by the need of relating physiological muscle activation and asymmetric VF vibration, our work introduces a novel approach through the asymmetric triangular body-cover model. This model explores imbalanced activation between the left- and right-side intrinsic laryngeal musculature, providing a more comprehensive understanding of vocal asymmetry in terms of clinical descriptions (Desjardins *et al.*, 2022). The proposed model mimics the triangular shape of the glottis and the layered structure of VF tissue, and has been integrated into a physiological vocal synthesizer, accounting for physical interactions both at the glottal level and along the vocal tract.

This work comprises distinct components, detailed in the subsequent sections. Section II delineates the adaptation of a previous model for a twofold configuration, outlines model simulations, introduces asymmetry feature calculations, and presents two cases with high-speed camera videos for contrasting model responses with experimental data. Section III shows the results obtained through the proposed model and compares them with the asymmetries from the experimental data. Section IV offers a thorough discussion of the findings and Sec. V concludes the manuscript.

II. METHOD

A. Asymmetrical triangular body-cover model

The triangular body-cover model (TBCM) (Alzamendi *et al.*, 2022), a symmetrical low-order model of the VFs, serves as the foundation for our asymmetric triangular body-cover model (a-TBCM). The TBCM incorporates tissue-fluid-acoustic interactions at the glottis, enabling simulations of sustained vowels and time-varying glottal gestures.

Building upon prior efforts in low-order modeling (Titze and Story, 2002), VF posturing (Titze and Hunter, 2007), body-cover VF models (Story and Titze, 1995), and the triangular shape of the glottis (Birkholz *et al.*, 2011), the TBCM consists of paired three-mass body-cover systems and a muscle-controlled model of all five intrinsic laryngeal muscles: cricothyroid (CT), thyroarytenoid (TA), lateral cricoarytenoid (LCA), interarytenoid (IA), and posterior cricoarytenoid (PCA). The LCA and IA muscles work synergistically to adduct the glottis, jointly medializing the VFs and closing the posterior gap, to initiate and sustain the phonation. The PCA muscle abducts the VFs, moving them apart, thus opening the glottal gap and facilitating the air flow through it, e.g., for breathing or coughing. Additionally, the CT muscle is the primary responsible for tensing and elongating the VFs during phonation, increasing pitch; whereas the TA muscle compresses and shortens the vocal folds, lowering pitch. The action of intrinsic laryngeal muscles in the larynx is represented in Fig. 1.

Considering the effects of the activation of the five intrinsic muscles allows for dynamic control of the prephonatory posture (i.e., vocal process accommodation: abduction level x_{02}, y_{02}, vocal fold length L_g, and thickness T) and the VF configuration (i.e., viscoelastic VF properties: masses m, springs k, and dampings d parameters) during phonation. Each intrinsic muscle is simulated using a modified Kelvin model for the stress-strain response in the tissues, considering both the passive and active stress components (Hunter *et al.*, 2004). The model offers flexibility by allowing normalized (beween 0 and 1) individual actuation levels for each muscle, namely, $(a_{\mathrm{LCA}}, a_{\mathrm{IA}}, a_{\mathrm{PCA}}, a_{\mathrm{CT}}, a_{\mathrm{TA}})$. Moreover, the TBCM allows for the incorporation of pulmonary pressure (P_L) as an adjustable input parameter, working in tandem with the muscle activation profiles.

In TBCM, the elastic, damping, and collision forces over the body-cover masses are computed following Galindo *et al.* (2017), while aerodynamic forces over the VF cover layer are computed according to Titze (2002). Glottal airflow is computed from the difference between subglottal and supraglottal pressure, and the glottal area, following Lucero and Schoentgen (2015). The acoustic wave propagation is simulated using the wave reflection analog scheme, modeling subglottal and supraglottal tracts as a discrete concatenation of acoustic cylinders with variable cross-sectional areas (Zañartu *et al.*, 2007). The TBCM implementation is summarized in Alzamendi *et al.* (2022).

The a-TBCM extends the TBCM, it is constructed around the coupling between two independent muscle-controlled TBCMs, as illustrated in Fig. 2, representing the left and right VFs. In this scheme, two muscle activation vectors are defined,

$$\vec{a}_i = [a_{\mathrm{IA}}, a_{\mathrm{LCA}}, a_{\mathrm{PCA}}, a_{\mathrm{TA}}, a_{\mathrm{CT}}]_i, \quad i \in \{\mathrm{L}, \mathrm{R}\}, \tag{1}$$

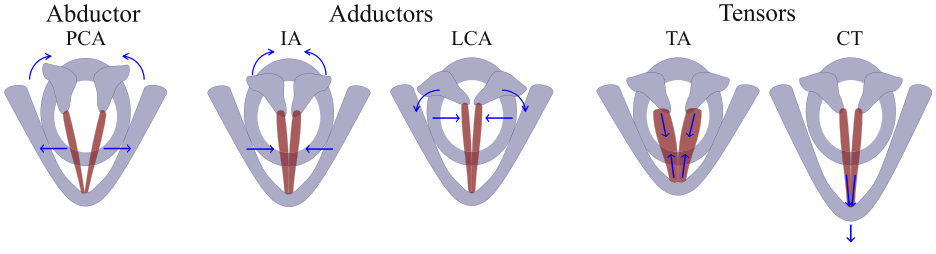

FIG. 1. (Color online) Effects of the five intrinsic muscle in glottal posture. Adapted from Titze and Hunter (2007) J. Acoust. Soc. Am. **121**(4), 2254, with permission of Acoustical Society of America. Copyright 2007 Acoustical Society of America.

https://doi.org/10.1121/10.0028164

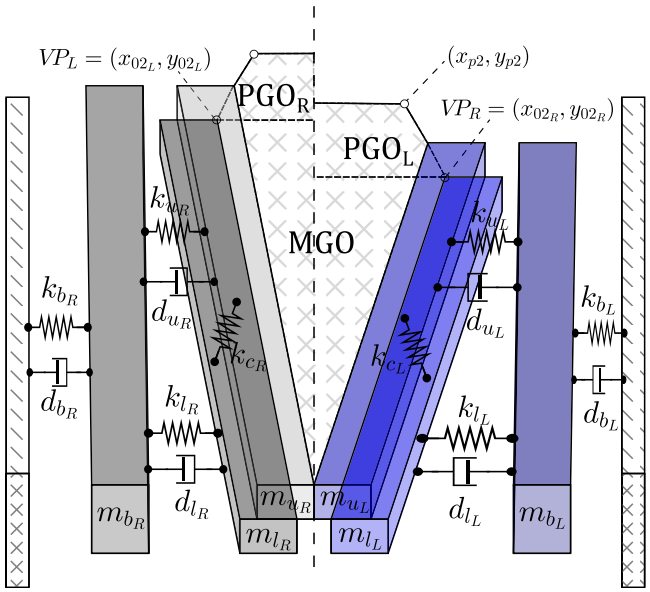

FIG. 2. (Color online) Schematic diagram of the VF configuration according to the a-TBCM for an abducted glottal configuration and asymmetrical muscle activation. The scheme shows the following: The vocal process (VP) defined by its position on the x and y axes (x_{02}, y_{02}). The position of the posterior wall (x_{p2}, y_{p2}). The posterior (*PGO*) and membranous (*MGO*) portions of glottal opening. Lumped mechanical components of mass (m), spring (k) and damper (d); for the upper (u), lower (l) and body (b) blocks; for the left (L) and right (R) vocal fold.

where the subscript i denotes the side of the a-TCBM, with L and R denoting left and right, respectively. The differences in VF geometry and mechanical components in a-TBCM, as shown in Fig. 2, are due to different muscle activation vectors on each side. Equal left/right activation vectors correspond to the symmetric control scheme in the TBCM. Then, the posture and the viscoelastic properties for left- and right-sided VF are determined by two muscle activation conditions. To model the dynamics of the VF, i.e., the movement of the body-cover elements, it is necessary to formulate and solve the coupled equations of motion for the left and right VF. For this, it is required a new way to calculate quantities such as glottal area, aerodynamic force, and collision force, that accounts for not having mirror symmetry or symmetric VFs (see Appendix A).

B. Muscle imbalance for a-TBCM: Bilateral posture and viscoelasticity

Muscle imbalance refers to a slight difference in the activation of the laryngeal muscles between the left and right VF. These varying muscle activations serve as inputs to the control mechanism, influencing the mechanical and geometric properties of the VF. The proposed a-TBCM provides a platform to explore the impact of imbalanced activation in the intrinsic musculature on the geometric and viscoelastic properties, influencing VF oscillations and the aerodynamics of glottal airflow. To establish a reference activation condition for the intrinsic laryngeal muscles, a simplification was introduced. The activation levels of the primary adductors (LCA and IA muscles) were combined by setting $a_{\mathrm{LCA}} = a_{\mathrm{IA}}$, streamlining the adjustable variables for sustained VF oscillations. Additionally, the PCA activation (a_{PCA}) was consistently set to zero across all simulations, neutralizing its significant abductor effect on glottal posture. For the TA and CT muscles, activations a_{TA} and a_{CT} were calibrated to produce voiced sounds within the fundamental frequency range of 90 to 100 Hz, aligning with the physiological characteristics of a male modal voice. The activation levels were determined based on muscle activation plots reported in Alzamendi *et al.* (2022). The reference activation for the right side is represented by

$$\vec{a}_R = [0.6, 0.6, 0.0, 0.6, 0.2]. \tag{2}$$

To represent the imbalance during voiced phonation, an asymmetry factor $q \in [0.5, 1.5]$ is introduced between the left and right sides in the a-TBCM. A similar idea has been previously applied by Steinecke and Herzel (1995), henceforth SH95. However, rather than controlling asymmetries in the mass-spring elements through a gain parameter as in SH95, the a-TBCM applies the asymmetry factor directly to the muscle activation levels. These levels jointly influence the posture and configuration of the VF. For comparison with other fold asymmetry approximations, the equivalent of SH95 for the TBCM model is implemented, where

$$m_L = \frac{m_R}{q}, \quad k_L = q k_R. \tag{3}$$

The modified masses and springs correspond to those presented in Fig. 2, representing the upper, lower, and body blocks. Two primary scenarios of muscle imbalance were explored: an asymmetric activation predominantly affecting glottal adduction (vocal process) and an asymmetry in the biomechanical properties (mass-spring values) of VF. To represent the first case, the asymmetry factor q was applied to a_{LCA} and a_{IA} in the left VF. The muscle activation vector for the left VF is then given by

$$\vec{a}_L = [q \cdot 0.6, q \cdot 0.6, 0.0, 0.6, 0.2]. \tag{4}$$

For asymmetries in the biomechanical properties, q was applied to a_{CT} and a_{TA} simultaneously, considering the CT-TA antagonistic relationship in determining the viscoelastic (VE) properties in the VF. The muscle activation vector for the left VF in this scenario is expressed as

$$\vec{a}_L = [0.6, 0.6, 0.0, q \cdot 0.6, q \cdot 0.2]. \tag{5}$$

Additionally, individual muscle imbalance in each CT and TA was studied separately, given its significance in characterizing the glottal configuration (Chhetri *et al.*, 2014a; Chung *et al.*, 2024). This resulted in a total of four configurations of muscular imbalance and the direct imbalance in masses and springs. The simulations were performed with a driving pulmonary pressure of 1 kPa. A truncated Taylor-series approximation was implemented to simultaneously solve the differential equations of motion for the six

masses, using a sampling frequency of 44.1 kHz. Vocal tract area function corresponding to an /i/ vowel (Story, 2008) was considered in order to closely match the experimental, the sustained /i/ sound brings a better access of the endoscope to the glottis. The subglottal tract was modeled as an inverted cone shape (Zañartu *et al.*, 2014).

C. Model derived measures

Several measures were derived from a-TBCM simulations to establish differences between the muscle imbalance scenarios, study the effect of the asymmetric factor on VF vibratory asymmetries, and compare the model with certain clinical cases. These measures include left-right amplitude asymmetry (*AA*), left-right phase asymmetry (*PA*), fundamental frequency (f_o), and open quotient (*OQ*). Following Mehta *et al.* (2011), synthetic kymograms were generated from the right and left VF edge positions over time, as illustrated in Fig. 3. Based on these representations, measures of the VF oscillatory asymmetries can be defined,

$$AA = \frac{A_R - A_L}{W}, \tag{6}$$

$$PA = \frac{t_L - t_R}{OP}. \tag{7}$$

Note that the normalization factor *OP* for defining PA follows that of Mehta *et al.* (2011), where the focus is on the acoustic effects generated during the open phase. These measures assess different aspects of oscillatory asymmetries. The left-right amplitude asymmetry, Eq. (6) (Qiu *et al.*, 2003), is the ratio between the difference and the sum of the maximum excursions for the right (reference) and left (affected) VF amplitude traces within one vibration period. The left-right phase asymmetry, Eq. (7) (Bonilha *et al.*, 2008; Lohscheller *et al.*, 2008), is the time delay between the maximum excursions of the left and right VF normalized by the open phase period.

The open quotient is computed from the kymogram as the quotient between the duration of the open phase (OP) and the period (P) for each cycle,

$$OQ = \frac{OP}{P}. \tag{8}$$

D. Clinical cases

In conjunction with the modeled scenarios, this study draws support from *in vivo* high-speed video (HSV) recordings representing voice disorders. Data for two female patients aged 25 to 30 years, one with non-phonotraumatic vocal hyperfunction (muscle tension dysphonia) and another with unilateral VF paralysis were included. During data acquisition, participants produced a sustained /i/ vowel sound at comfortable pitch and loudness levels. Before data recording, the participants adhered to informed consent procedures and Institutional Review Board protocols outlined in FONDECYT 1151077 project.

The HSV data collection involved an advanced high-speed camera (SA-X2, Photron, Tokyo, Japan) synchronized with a rigid endoscope (9106, KayPentax, Montvale, NJ) equipped with a 35 mm C-mount adapter and a xenon light source (7152B, KayPentax, Montvale, NJ). The HSV dataset, comprising approximately 2670 frames at 8000 frames per second (fps), underwent pre-processing. This included selecting 600 frames and identifying a 256×256 pixel region of interest containing only the VFs. The refined HSV dataset was then used to segment the glottis area using GlottalImageExplorer (Birkholz, 2016).

Subsequent to the glottis area segmentation, the digital kymogram (DKG) technique proposed by Mehta *et al.* (2011) was applied to visualize VF trajectories. These lateral displacement waveforms, capturing intricate motions of the left and right VFs, were traced along a one-pixel line positioned at the midpoint of the glottal region's posterior-anterior length. Additionally, the DKG outputs facilitated the automated extraction of amplitude and phase asymmetry metrics for the left and right VFs.

To represent female phonations, geometric quantities of the model were adjusted following Titze and Story (2002). Specifically, the resting length (L_g) of the vocal fold was reduced from 16 to 10 mm, the resting thickness (T_g) from 3 to 2 mm, the ligament depth from 20 to 15 mm, the mucosal depth from 20 to 15 mm, and the muscle depth from 40 to 30 mm. Additionally, the model was coupled with a female /i/ tract, utilizing the area function outlined in Story *et al.* (1998).

III. RESULTS

A. Influence of muscle imbalance on VF properties

To illustrate the change in the mechanical properties of the VFs due to the muscle imbalance, Fig. 4 shows the effect

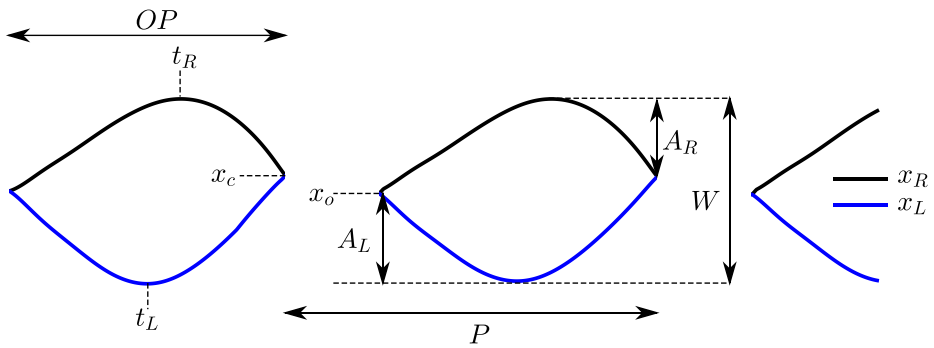

FIG. 3. (Color online) Kymogram parametrization: x_L, x_R displacement of left/right VF; t_L, t_R time of maximal left/right VF displacement; x_c, x_o mediolateral position of VFs at the glottal closure/opening; A_L, A_R maximum displacement of left/right VF; W peak-to-peak glottal width; P glottal period; and OP open phase. Adapted from Mehta *et al.* (2011) J. Acoust. Soc. Am. **130**(6), 3999–4009, with permission of Acoustical Society of America. Copyright 2011 Acoustical Society of America.

https://doi.org/10.1121/10.0028164

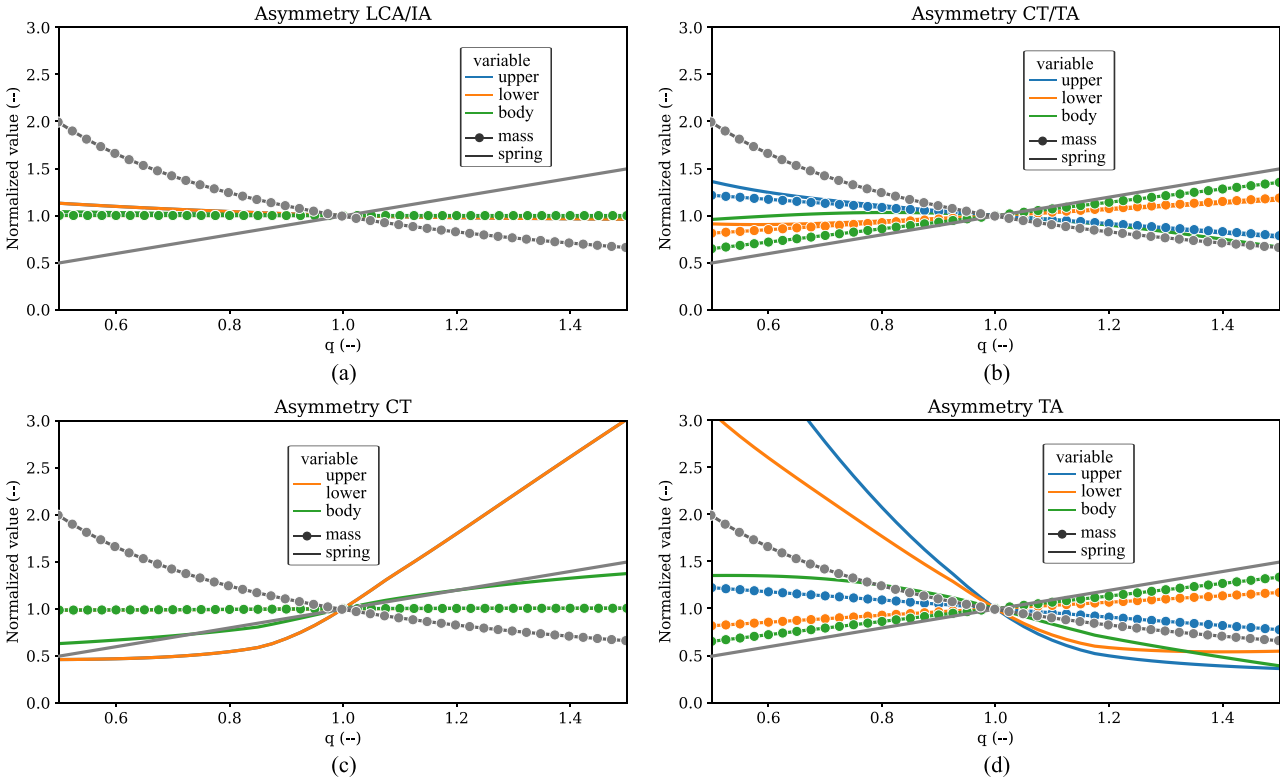

FIG. 4. (Color online) Effects on normalized (pointed line) masses and (solid line) springs when varying the joint asymmetry factor q for LCA/IA (a), CT/TA (b) configurations, and single asymmetry in CT (c) and TA muscle (d). The legend represents the nomenclature in a-TBCM scheme (see Fig. 2, and Table III) for mass m, and spring k: upper u, lower l, and body b blocks. The gray color describes the effects due to the asymmetry mechanism introduced in SH95.

of q on the values of the masses (pointed lines) and springs (solid lines) of the three blocks (upper, lower, and body) that compose the VFs, for the four different cases of imbalance described in the method. The effect in mass and spring is represented by the normalized value of these parameters, such normalization is made with respect to the value in the balanced case ($q = 1$). In addition, the asymmetry mechanism introduced in SH95 is included in gray color for comparison.

As shown in Fig. 4(a), the asymmetry in the adductor muscles (LCA/IA), has a negligible impact on the mass of the blocks, pointed lines, but leads to a minor alteration ($<10\%$) in all the elastic component, solid lines. This is due to the relatively minor role that adductor muscles play in the construction of the folds, although they do contribute slightly to their elongation.

For the stiffness component, the solid lines in Figs. 4(c) and 4(d), the imbalance in the CT muscle produces a trend in the same direction as the SH95 reference mechanism, k increasing with q, although not in a strictly linear manner in the cover component, orange line. Conversely, the imbalance in the TA muscle produces an effect of decreasing stiffness with increasing q, opposite to the SH95 reference mechanism and the imbalance in the CT muscle.

Regarding the mass component, the pointed lines in Figs. 4(c) and 4(d), imbalance in the CT muscle does not lead to any changes. However, an imbalance in the TA muscle results in a linear change in the mass of the body block, green dots, and redistributes the mass of the cover between the upper and lower blocks, blue and orange dots. This pattern contradicts the direct imbalance in mass and spring values and highlights the intricacy of the laryngeal control mechanism. The CT muscle elongates the fold, impacting its elasticity without adding any mass. In contrast, the TA muscle is responsible for adding mass to the fold and redistributing it between the blocks by altering their dimensions. This generates an effect on both the mass and spring components. Similar trends are described in the work of Titze and Story (2002), where the mechanism we used to calculate masses and springs from muscle activation is explained.

The joint imbalance in CT and TA, Fig. 4(b), shows the pondered effect of the individual imbalances. The spring component, solid lines, is the sum of the opposing effects, resulting in a decreasing effect with q of small magnitude. The mass component, pointed lines, is the same as in the imbalance in TA, since the imbalance in CT has no effect on the mass of the blocks.

Figure 5 illustrates the impact of q on fundamental frequency (f_o) and posterior glottal opening (PGO) in various imbalance scenarios. Notably, the configuration with an imbalance in LCA and IA muscles exhibits a non-zero posterior gap, resulting in an increased PGO for $q < 1$. This effect arises from the action of the LCA and IA muscles in

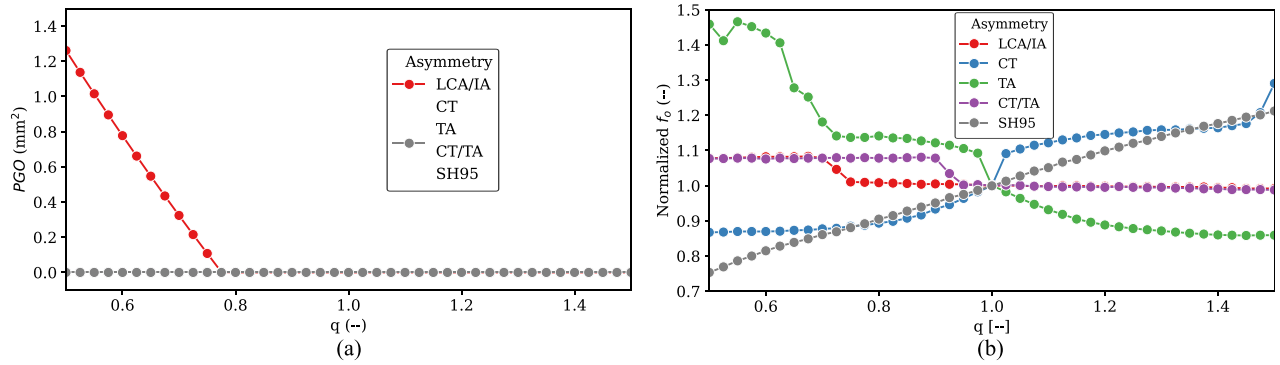

FIG. 5. (Color online) Effects on *PGO* (a) and f_o (b) when varying q for muscle imbalance configurations. SH95 results shown for comparison.

adducting the VFs. In contrast, other imbalance scenarios do not induce changes in *PGO* due to a lack of alteration in the adduction degree of the folds. For instance, the SH95 approach, which does not consider vocal posture, exhibits no *PGO* changes.

Upon examining the influence of the q factor on fundamental frequency, distinct behaviors emerge in comparison to the SH95 model. Similar to Fig. 4, Fig. 5(b) shows f_o normalized to the balanced case ($q = 1$). In the SH95 model, the q factor proportionally affects f_o, reflecting its design intent. Conversely, in cases of muscle imbalance, different patterns are observed. An imbalance in the TA muscle leads to an inverse relationship with f_o—increasing q results in a decrease in f_o, influenced by the effect of TA on the VF spring. On the other hand, an imbalance in CT exhibits a slight direct correlation with f_o; an increase in q correlates with an increase in f_o, with a defined threshold for the minimum and maximum f_o values. In scenarios involving joint imbalance of two muscles, CT/TA and LCA/IA, the fundamental frequency displays a step-like behavior. At a specific point, there is a 10% variation in its value, indicating a transition between frequencies.

B. Influence of muscle imbalance on VF oscillation

To examine the impact of muscle imbalance on VF oscillation, Fig. 6 provides waveforms illustrating synthetic kymograms and glottal airflow. These visualizations encompass the baseline a-TBCM simulation and imbalance scenarios under two configurations: hypofunction ($q = 0.5$) and hyperfunction ($q = 1.5$). The first row displays a synthetic kymograph illustrating the amplitude displacements of the

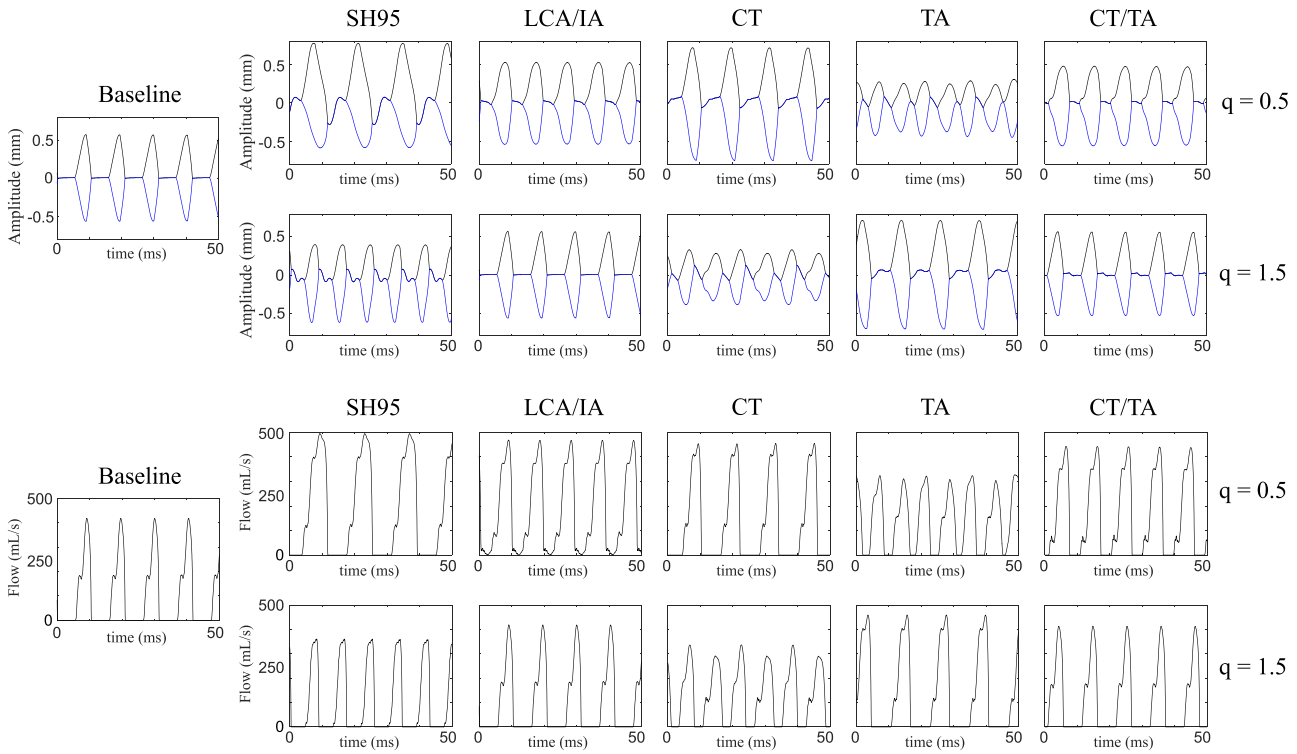

FIG. 6. (Color online) Comparison of kymograms and airflows from a-TBCM simulations for asymmetry scenarios and two imbalance conditions: hypofunction ($q = 0.5$) and hyperfunction ($q = 1.5$.).

https://doi.org/10.1121/10.0028164

TABLE I. Comparison of asymmetry values and oscillation features between the baseline and the q configurations shown in Fig. 6. For each feature, the first row is for the hypofunction ($q = 0.5$) and the second row is for the hyperfunction ($q = 1.5$).

	Baseline	SH95	LCA/IA	CT	TA	CT/TA
f_o (Hz)	96	72.4	103.6	83.4	140.2	103.5
		116.5	95.3	124	82.6	94.5
OQ (%)	49	60	66.5	51.8	78.7	68.4
		53.9	49.1	72.8	52	49.2
AA (%)	0	31.3	−1.5	−3.1	−21.5	−8.27
		−22.1	0.4	−8.7	−0.5	2.9
PA (%)	0	24.71	−1.9	18.2	−17.5	−5.8
		−21.5	0.44	−16.9	18.2	0.3

left and right VFs in millimeters. The second row presents glottal airflow expressed in milliliters per second. All signals correspond to a 50 ms simulation. Additionally, Table I furnishes computed asymmetry measures, including f_o, OQ, AA, and PA for the simulated scenarios.

In the context of direct mass and spring imbalance, as depicted in the second column of Fig. 6, the hypofunction configuration results in an increase in glottal area, indicated by an increase in airflow. Furthermore, the oscillation amplitude of the affected fold is smaller compared to the unaffected fold, leading to an AA value exceeding 30%. A positive PA value, surpassing 20%, is also evident, accompanied by a decrease in the fundamental frequency during oscillation. In the hyperfunction configuration, this displacement behavior is reversed. Now, the affected fold undergoes greater displacement, reaching its maximum value first, accompanied by an increase in frequency and a decrease in flow amplitude.

In the case of imbalance in the LCA/IA adductor muscles, hypofunction exhibits a slight increase in maximum airflow, along with asymmetry measurements AA and PA below 2%. These measurements indicate that the less adducted (modified) fold exhibits greater displacement. A notable observation in this case is the nonzero airflow value during the closed phase of VF oscillation, aligning with the nonzero PGO value reported in Fig. 5. In the hyperfunctional configuration, this asymmetry maintains the baseline shape, as, after a certain level of activation in LCA and IA, the folds are already parallel. Therefore, an increase in muscle activation does not induce visible changes in the glottis with asymmetry measures below 1%.

For individually applied CT and TA muscle imbalance, a cross-behavior is observed in terms of hypofunction and hyperfunction. In the case of altered CT muscle activity, displacements comparable to the baseline are observed in hypofunction, with greater displacement of the affected fold ($AA = -3\%$) and reduced amplitude oscillation for the hyperfunctional condition. Conversely, in TA imbalance, the reduced amplitude of the folds occurs in hypofunction, while oscillation similar to the baseline is observed in hyperfunction. This underscores the antagonistic nature of this muscle pair in the viscoelastic composition of the VFs, as also observed in the mass and spring curves presented in Fig. 4. This cross-behavior is clearly evident in the OQ, f_o, and PA values presented in Table I. For individual muscle imbalance, positive values for AA are unattainable, signifying that the affected muscle has a greater amplitude of oscillation.

In terms of VF oscillation behavior, Fig. 7 demonstrates the influence of the asymmetry factor q on AA and PA across the examined cases. The conventional imbalance scheme, SH95, yields positive values for AA and PA when $q < 1$, indicating that the affected fold's oscillation is dampened due to an increase in mass and a decrease in elasticity. Conversely, it intensifies its oscillation and frequency, resulting in negative values of AA and PA for $q > 1$.

When considering scenarios of muscle imbalance, several significant observations emerge. The imbalance in CT mirrors the conventional scheme's trend for PA, while the imbalance in TA exhibits the opposite trend. This discrepancy can be attributed to the behavior of the elastic component as a function of the q factor, increasing in the CT imbalance and SH95, and decreasing in the TA imbalance. Regarding AA, it proved challenging to find a muscle imbalance scenario that generated the same range as the reference scheme. This stems from the mechanism of muscle activation control and the mass and spring parameters, where not all mass values move in the same direction when varying muscle activation.

In contrast, the imbalance in LCA/IA yields the most minor effect on asymmetry measurements within the studied

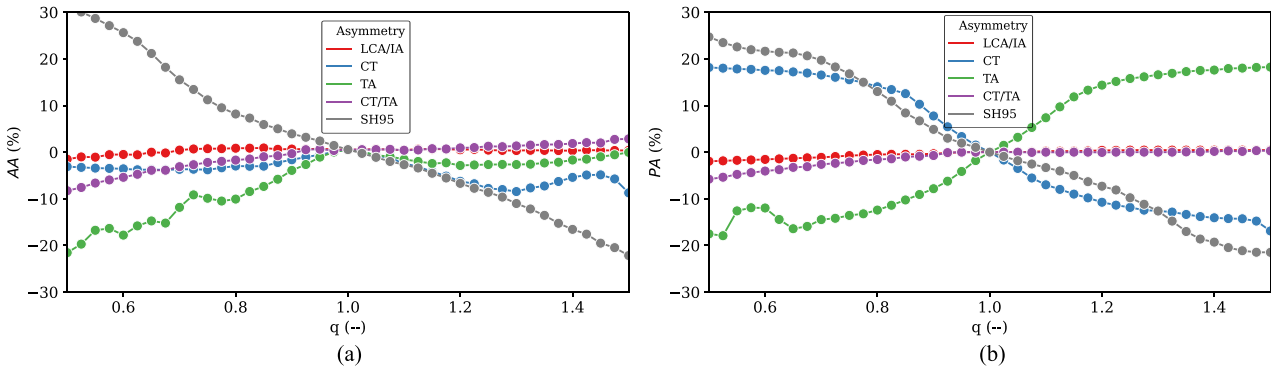

FIG. 7. (Color online) Effect of changing q on asymmetry metrics; AA (a) and PA (b), for the different imbalance approaches.

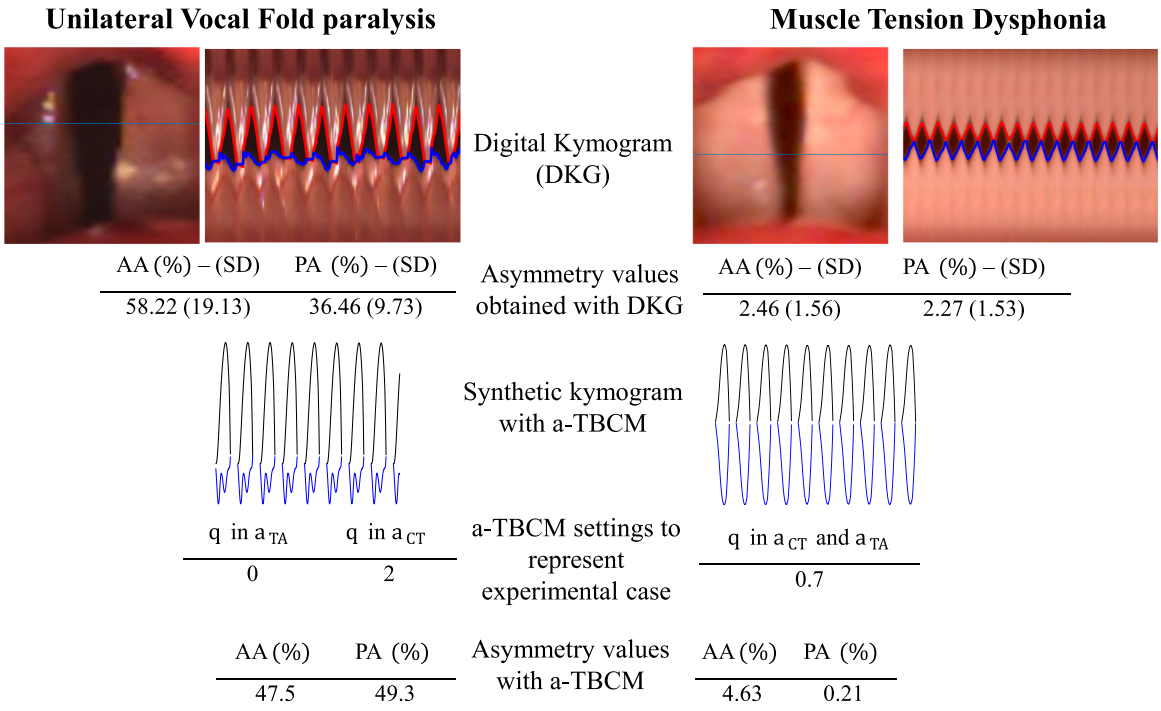

FIG. 8. (Color online) Comparison of clínical (HSV and DKG) data and the corresponding simulated responses using a-TBCM: (left) Unilateral VF paralysis and (right) muscle tension dysphonia.

range, resulting in asymmetries of less than 2%. Meanwhile, the combined imbalance of CT/TA amalgamates the effects of individual imbalance, producing phase asymmetries of approximately 6% and amplitude asymmetries approaching 10%.

C. Contrasting a-TBCM against *in vivo* examples

To demonstrate the efficacy of incorporating muscle imbalance in modeling various clinical scenarios, we present clinical HSV images alongside simulated data generated using the a-TBCM in Fig. 8. This illustration highlights two distinct cases: unilateral VF paralysis (left) and muscle tension dysphonia (right). Each case features the DKG derived from clinical data, juxtaposed with the synthetic kymogram produced by the a-TBCM. Synthetic DKGs were generated by adjusting *AA* and *PA* measurements heuristically to align with their respective clinical mean and variance values, employing the muscle activation defined in Eq. (5) as the baseline. The simulation process encompasses the insights detailed in the preceding subsections, accounting for the characteristic oscillatory behavior associated with each pathology. Specifically, for VF paralysis, our aim was to emulate a rigid VF, while for muscle tension dysphonia, we introduced a subtle differentiation between the VFs.

Once the mechanism of muscle imbalance was defined for each case: joint imbalance in CT and TA for dysphonia, and TA off and hyperfunction in CT for paralysis; the parameter q for baseline muscle activation was swept with a step of 0.1 in a range from 0 to 2 and the simulation closest to the *AA* and *PA* values of the experimental data were taken.

Figure 8 highlights the specific imbalance factors employed in generating the synthetic kymogram, providing clarity on the value of q and the muscle to which it is applied. It is worth noting that while this approach may not be entirely singular, a more precise representation could potentially be achieved through model optimization considering the complete kymogram signal. Nevertheless, in both cases, the a-TBCM successfully produces a waveform closely mirroring the actual kymogram. In the instance of VF paralysis, this results in a fold with minimal amplitude oscillation, out of phase in time. In the case of muscle tension dysphonia, it yields a slightly asymmetric oscillation in both amplitude and phase.

Figure 8 also presents corresponding *AA* and *PA* measurements from both clinical and synthetic data. Clinical assessments of VF oscillatory asymmetry display noteworthy variability, emphasizing their sensitivity to spatiotemporal resolution and the challenges in obtaining precise measurements of this nature. In the case of unilateral paralysis, both *AA* and *PA* values surpass 30%, indicating substantial asymmetry. These asymmetry values are effectively captured by the a-TBCM, which deactivates the TA in the paralyzed fold. Similarly, in the case of muscle tension dysphonia, the a-TBCM enables the representation of such levels of asymmetry by introducing an activation imbalance in the CT and TA simultaneously.

IV. DISCUSSION

The primary aim of this study was to introduce and demonstrate the concept of muscle imbalance as a mechanism for inducing asymmetries within the VFs. We sought

https://doi.org/10.1121/10.0028164

to establish its potential in characterizing clinical scenarios by examining the influence of intrinsic laryngeal muscles on the glottis and drawing comparisons with previous approaches for understanding asymmetric VF oscillations.

Our findings lead us to conclude that achieving a direct differentiation scheme akin to SH95 through an imbalance in a single muscle alone is not feasible. The closest approximation is attained through an imbalance in the CT muscle. Additionally, the antagonistic relationship between the CT and TA muscles hinders the replication of the direct imbalance scheme. However, introducing imbalance in both these muscles concurrently, albeit in opposite directions with proportional imbalance in CT and inversely proportional in TA, appears to be a promising avenue towards achieving an analog of the conventional asymmetry mechanism using muscle imbalance. It is worth noting that a comprehensive exploration of this intricacy exceeds the scope of this initial study.

The proposed method for prescribing muscle imbalance provides a systematic means to introduce asymmetry in the composition and positioning of the VFs. This asymmetry has been studied independently by other researchers. Prior efforts (Dresel *et al.*, 2006; Jiang *et al.*, 2006; Mehta *et al.*, 2011; Xue *et al.*, 2010) report ranges of amplitude and phase asymmetry akin to our findings. Conversely, studies such as Dresel *et al.* (2006), Samlan and Story (2017), and Samlan *et al.* (2014) report differentiation in the vocal process without altering the mechanical properties of the VFs, resulting in increased minimum glottal flow and decreased sound pressure, much like the effects observed with the imbalance in the LCA and IA adductor muscles.

When considering the results of mechanical parameters and asymmetry measurements collectively, it becomes evident that phase asymmetry aligns with the spring component trends, while mass trends are associated with amplitude asymmetry. This elucidates why the imbalance mechanism does not yield significant amplitude values. Each block follows a distinct mass pattern when subjected to imbalance, resulting in a small *AA* that deviates from the SH95 scheme, where all blocks experience similar mass effects.

The clinical examples presented in this study serve to illustrate the potential of our approach in emulating actual cases, thereby enhancing our understanding of the origins of differences in VFs, be it in cases of vocal cord paralysis (Ivey, 2019; Tipton *et al.*, 2020) and primary muscle tension dysphonia (Hsiung and Hsiao, 2004; Spencer, 2015). While similar insights may exist within other methodologies, our approach integrates muscular activity directly, impacting glottal configuration. For instance, paralysis is depicted as an inert and minimally mobile fold, whereas further variations showcase a fold with high mass and rigidity. Notably, this work represents an initial foray into a parameter fitting and optimization problem, without delving into extensive details. Our objective is to demonstrate the utility of this imbalance approach, as exemplified in Fig. 8.

The standard deviation in the measurement of the symmetry features for the clinical cases presented in Fig. 8, show how sensitive the oscillation of the vocal folds is. This can be attributed to the vocal gesture /i/ performed by the subjects, since it has a formant with a low frequency, which increases the interaction between the vocal tract and the glottis due to the proximity of the tract resonance and the fundamental frequency (Wade *et al.*, 2017; Zañartu *et al.*, 2011; Zhang, 2018).

Studying VF oscillation with diverse properties presents several challenges, including the presence of harmonics, as illustrated in Fig. 6, a topic extensively explored by other researchers (Sommer *et al.*, 2013; Steinecke and Herzel, 1995; Zhang and Jiang, 2004). In addition, the a-TBCM has some limitations. This model is a simplified approach to VFs that uses a lumped element approach where one continuous block represents the entire anterior-posterior direction. This approach does not allow the assignment of different oscillation patterns to the anterior, medial, and posterior portions of the VF, where other studies have shown different degrees of asymmetry (Bonilha *et al.*, 2012; Malinowski *et al.*, 2024). For an extensive validation of this type of model, a critical consideration is the impact of the chosen reference point, whether it pertains to muscular activation or the specific values assigned to masses and springs.

On the other hand, the muscle imbalance postulate presents a greater challenge for its experimental validation. A first level of validation could be done by experiments with excised larynxes. In this area, there are several works that study the action of the laryngeal muscles on the elongation and posture of the VFs (Chhetri *et al.*, 2014b; Chhetri and Park, 2016; Döllinger *et al.*, 2016). A possible experiment would be the asymmetric stimulation of the larynx to measure the differences in left and right oscillation, a setup like the one presented in Schlegel *et al.* (2022), where unfortunately the video analysis is done from the glottal area wave (GAW) and not from the kymogram. The next level of validation would be with intramuscular electromyography. Here, there are few works that present the action of the laryngeal muscles, and this has been done symmetrically (Hillel, 2001; Poletto *et al.*, 2004).

Ongoing efforts measure simultaneously the activity of the left and right TA and CT with intramuscular EMG and HSV of the larynx to associate muscle imbalance with asymmetries in vocal fold oscillation, and contrasting with asymmetric VF silicone model. Therefore, future efforts will include the integration of clinical knowledge and new experimental data to ensure the accuracy of predictions and trends generated by models representing asymmetric VF oscillations.

V. CONCLUSION

This study introduces a muscle-controlled, triangular and asymmetrical body-cover model of the VFs to explore the impact of muscle imbalance on VF vibration. The findings reveal significant alterations in the dynamics of mass-spring and modulation of fundamental frequency when comparing activation-based muscle imbalance to conventional methods. The incorporation of muscle activation as a distinguishing factor in VF composition has the potential to

revolutionize our comprehension of vocal asymmetry. This shifts the focus beyond mere structural considerations, emphasizing the critical role of muscular coordination. Moreover, initial experiments have successfully replicated clinical scenarios of VF paralysis and muscle tension dysphonia. However, further research is imperative to comprehensively assess the proposed muscular imbalance descriptions in clinical settings. Nevertheless, this study makes a significant contribution to advancing our understanding of VF dynamics and highlighting the pivotal role of muscle imbalance in normal and disordered voice production.

ACKNOWLEDGMENTS

This research was supported by the National Institutes of Health (NIH) National Institute on Deafness and Other Communication Disorders Grant No. P50 DC015446, ANID grants Becas de Doctorado Nacional Grants Nos. 21202490 and 21190074, FONDECYT Grant No. 1230828, BASAL Grant No. FB0008, UTFSM grant DPP PIIC No. 077/2022, and Corporación Universitaria Iberoamericana, Research Department, under search grant for project 202210D038. The content is solely the authors' responsibility and does not necessarily represent the official views of the NIH.

AUTHOR DECLARATIONS

Conflict of interest

Carlos Calvache has financial interests in Vocology Center, a company focused on vocal rehabilitation processes, professional voice training, and continuing education in the field of spoken, sung, and interpreted voice. Carlos Calvache's interests were reviewed and are managed by Corporación Universitaria Iberoamericana, Bogotá, Colombia, in accordance with its conflict-of-interest policies. Matías Zañartu has financial interest in Lanek SPA, a company focused on developing and commercializing biomedical devices and technologies. Matías Zañartu's interests were reviewed and are managed by Universidad Técnica Federico Santa María in accordance with its conflict-of-interest policies.

DATA AVAILABILITY

The data that support the findings of this study are available from the corresponding author upon reasonable request.

APPENDIX A: IMPLEMENTATION OF THE ASYMMETRICAL TRIANGULAR BODY-COVER MODEL

The proposed a-TBCM is an extension of the TBCM (Alzamendi *et al.*, 2022) and builds upon prior efforts (Birkholz *et al.*, 2011; Galindo *et al.*, 2017; Story and Titze, 1995; Titze and Hunter, 2007; Titze and Story, 2002). The proposal moves from a symmetrical to an asymmetrical glottal configuration considering the left and right VFs with two VFs with their independent muscle activation vector.

1. Posture and biomechanical properties

For each side of the a-TBCM, as shown in Fig. 2, the dynamic adjustment of vocal posture and VF configuration as a function of activation vector $\vec{a}_i$ in Eq. (1) follows the methodology in the TBCM. The theoretical development and the implementations were described in Alzamendi *et al.* (2022) and Galindo *et al.* (2017), and are briefly summarized for completeness.

A system of equations of motion models the laryngeal posturing by describing the relative movements between the arytenoid cartilage and the cricoid cartilage, and between the cricoid cartilage and the thyroid cartilage, in response to the forces in the laryngeal tissues. Vocal process Cartesian coordinates are tracked, and from this information and the forces in the laryngeal tissues, the adductory displacements, $\Delta x_{u,i}, \Delta x_{l,i}$, and the VF lengths, L_i, for $i \in \{L, R\}$ are obtained (see Fig. 9).

Thereupon, empirical rules are applied for adjusting the geometrical and biomechanical parameters (Alzamendi *et al.*, 2022) [e.g., thickness, depth, and mass m for each block, the nodal point, the glottal convergence, and the values for the spring k and damping d parameters (see Fig. 2)] of the left/right TBCM.

2. Glottal areas calculation

The total glottal area A_g is the contribution of the membrane portion of the VFs (*MGO*) and the posterior gap (*PGO*), as shown in the Fig. 2.

In the a-TBCM, the *MGO* for upper or lower blocks is computed as follows:

$$A_m = A_{Tr_R} + A_{Tr_L} + A_{Rect}, \tag{A1}$$

where the subscripts indicate whether the area is triangular, *Tr*, or rectangular, *Rect*. For the computation of these areas, the fraction of the block that is under collision is introduced as a quantity that simplifies the expressions (Galindo *et al.*, 2017),

$$\alpha_i = \max\left(0, \min\left(\frac{y_{col}}{L_i}, 1\right)\right), \quad i \in \{\mathrm{L}, \mathrm{R}\}. \tag{A2}$$

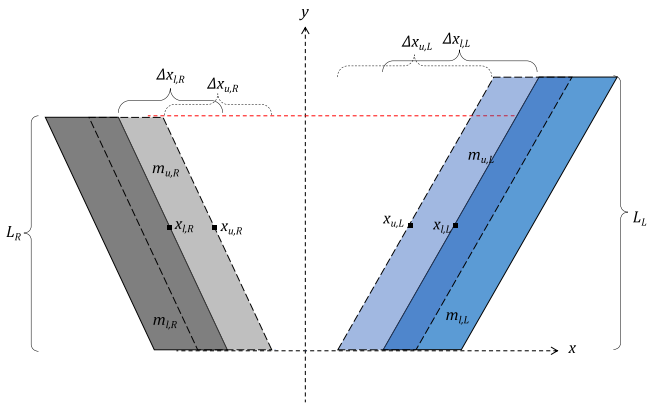

FIG. 9. (Color online) Top view: 2D diagram describing the abducted VFs positioning for the cover blocks in the a-TBCM.

https://doi.org/10.1121/10.0028164

The collision height y_{col} in Eq. (A2) denotes the y-coordinate of the point where the left- and right-edge lines intercept determines the collision height (see the red dot in Fig. 10). There are two possible scenarios for the glottis, as shown in Fig. 10 (top), VF in no collision: $(\alpha = 0)$, and (bottom) VFs in collision: $(\alpha > 0)$.

The triangular-shaped glottal area is calculated as follows:

$$A_{Tr_i} = (1-\alpha_i)^2 L_i \frac{\Delta x_i}{2}, \tag{A3}$$

where factor $(1-\alpha_i)$ is the non-collision portion of the VF, and the subscript $i \in \{L, R\}$. On the other hand, the rectangular-shaped area is obtained from

$$A_{Rect} = \max(0, x_{B_R} - x_{B_L}) \frac{L_R + L_L}{2}. \tag{A4}$$

Note that during VF collision, $A_{Rect} = 0$ in Eq. (A1).

The cross-sectional area, A_t, and the contact area, A_{col}, are obtained from the collision fraction, α_i, in a similar way as in Alzamendi *et al.* (2022),

$$A_{t_i} = (1-\alpha_i) L_i T_i, \tag{A5}$$

$$A_{col_i} = \alpha_i L_i T_i, \tag{A6}$$

where $i \in \{L, R\}$.

The posterior glottal opening, *PGO*, is defined for each VF following Alzamendi *et al.* (2022), using the cricoarytenoid junction coordinate. In the a-TBCM, the *PGO* is the contribution of both VFs,

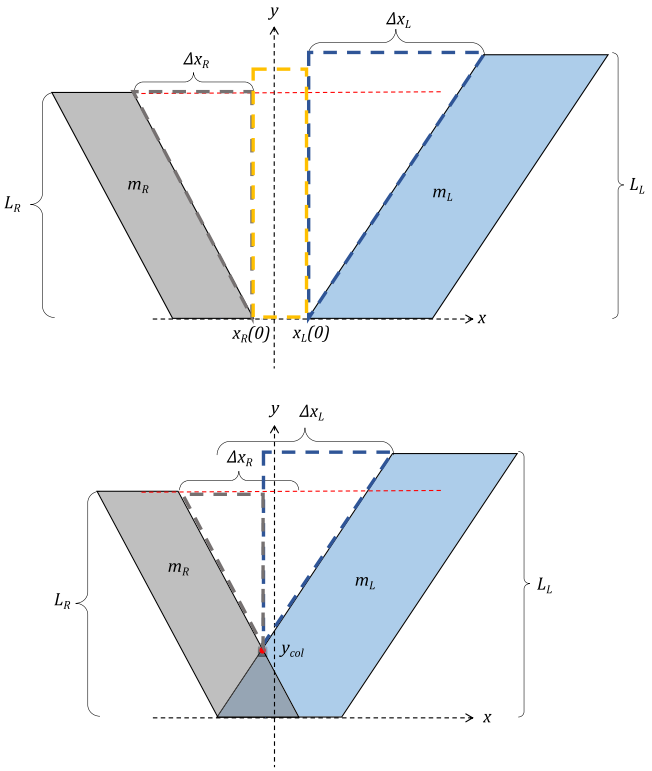

FIG. 10. (Color online) Glottal area scheme for VF blocks: (top) no collision, (bottom) collision.

$$PGO = PGO_R + PGO_L. \tag{A7}$$

The total glottal area is the sum of the membranous area and the posterior gap,

$$A_g = A_M + PGO, \tag{A8}$$

where $A_M = \min(A_{m_u}, A_{m_l})$, the minimum between upper and lower *MGO*, as shown in Fig. 9.

3. Equations of motion

The asymmetrical VF vibrations are simulated on the basis of coupled left/right systems of equations of motion. Each system simulates the medial-lateral displacements for the upper (u) and lower (l) cover masses and the body (b) mass in the TBCM (see Fig. 2).

The equations of motion for each VF are

$$m_{u,i}\ddot{x}_{u,i} = F_{k;u,i} + F_{d;u,i} - F_{k;c,i} + F_{e;u,i} + F_{col;u,i}, \tag{A9a}$$

$$m_{l,i}\ddot{x}_{l,i} = F_{k;l,i} + F_{d;l,i} - F_{k;c,i} + F_{e;l,i} + F_{col;l,i}, \tag{A9b}$$

$$m_{b,i}\ddot{x}_{b,i} = F_{k;b,i} + F_{d;b,i} - F_{k;u,i} - F_{d;u,i} - F_{k;l,i} - F_{d;l,i}, \tag{A9c}$$

where i denotes the considered side (L or R), m is the mass of the block and x is the medial-lateral displacement over time. The right side of the equation presents the net force acting upon the block due to elastic (k), damping (d), aerodynamic (e), and collision (col) components.

The elastic forces $(F_{k;u,i},\ F_{k;l,i},\ F_{k;c,i},\ F_{k;b,i})$ are modeled through a nonlinear Hooke's law, and the damping forces $(F_{d;u,i},\ F_{d;l,i},\ F_{d;b,i})$ are modeled proportional to the velocity. These force components are not affected by the presence of the other VF. The explicit equation for each force component can be found in the Appendix in Galindo *et al.* (2017).

The aerodynamic driving forces $(F_{e;l,i},\ F_{e;u,i})$ represents the force that the intraglottal pressure exerts on the VFs. It depends on the glottal flow, glottal and transversal area. Previous works explain how to calculate the intraglottal flow and pressure from the upper/lower glottal area (Story, 2008). Using the definition of pressure, the aerodynamic force for the upper/lower block is

$$F_{e;u,i} = P_{int;u}(A_g) \times A_{t_i}, \tag{A10a}$$

$$F_{e;l,i} = P_{int;l}(A_g) \times A_{t_i}, \tag{A10b}$$

where P_{int} is the intraglottal pressure (constant in the entire upper or lower block) which is a function of glottal area A_g and the sub- and supra-glottal pressures, and A_t is the cross-sectional area that multiplies the pressure to compute the force component, which depends on the geometry and collision fraction α of the VF. The equations from Galindo *et al.* (2017) are used to calculate the intraglottal pressure from

the glottal area; however, it is necessary to define how to calculate the glottal and cross-sectional areas in the a-TBCM due to the lack of mirror symmetry.

The collision forces ($F_{col;u,i}$, $F_{col;l,i}$) depend on the interpenetration distances in the upper/lower cover masses due to the impact between opposing VFs. Therefore, the computation of the collision force requires defining when the collision occurs, and the VF section undergoing the collision.

Similar to Galindo *et al.* (2017), the total collision force for the lower or upper blocks is

$$F_{col;j,i} = -k^*_{col;j} \int_0^{y_{col;j}} \left(d_{j,i}(y) + \eta_{col;j} d^3_{j,i}(y) \right) dy, \qquad \text{(A11)}$$

where $i \in \{\mathrm{L}, \mathrm{R}\}$, $j \in \{\mathrm{l}, \mathrm{u}\}$, $d(y)$ is the interblock penetration distance, y_{col} is the collision height, k^*_{col} is the effective spring collision constant, and η_{col} is a nonlinear coefficient. To calculate the interblock penetration distance $d(y)$, the VF edge is described as a straight line. The x position of the VF is a function of the y coordinate, as follows:

$$x_{j,i}(y) = b_{j,i} y + c_{j,i}, \quad i \in \{\mathrm{L}, \mathrm{R}\} \quad \text{and} \quad j \in \{\mathrm{l}, \mathrm{u}\}, \qquad \text{(A12)}$$

where b is the slope and c is the intercept, see below. The explicit values for quantities are obtained from Fig. 9 that shows a 2D top view of the cover masses, where L_i is the VF length, $x_{j,i}$ is the mass position and $\Delta x_{i,j}$ is posterior displacement, given the degree of abduction by the muscle activation,

$$b_{j,i} = \begin{cases} -\dfrac{\Delta x_{j,L}}{L_L} & \text{for} \quad i = L \quad \text{and} \quad j \in \{\mathrm{l}, \mathrm{u}\}, \\ \dfrac{\Delta x_{j,R}}{L_R} & \text{for} \quad i = R \quad \text{and} \quad j \in \{\mathrm{l}, \mathrm{u}\}, \end{cases} \qquad \text{(A13)}$$

$$c_{j,i} = \begin{cases} x_{j,L} + \dfrac{\Delta x_{j,L}}{2} & \text{for} \quad i = L \quad \text{and} \quad j \in \{\mathrm{l}, \mathrm{u}\}, \\ x_{j,R} - \dfrac{\Delta x_{j,R}}{2} & \text{for} \quad i = R \quad \text{and} \quad j \in \{\mathrm{l}, \mathrm{u}\}. \end{cases} \qquad \text{(A14)}$$

Without loss of generality, consider one of the cover elements, either upper or lower for both VFs; the upper or lower subscript is removed to have a short notation since the expression and the formulation is equivalent for both blocks. With the mathematical description of the VF edges in Eq. (A12), the interblock penetration distance is defined by

$$d_R(y) = x_R(y) - x_L(y), \qquad \text{(A15)}$$

note that $d_L(y) = -d_R(y)$, this denotes the opposite direction in collision forces. Additionally, this distance gives the collision condition:

$$d_R(0) \geq 0. \qquad \text{(A16)}$$

For the calculation of the collision height y_{col} in Eq. (A11), three possible glottal configurations are considered (see Fig. 11): the posterior portions in both VFs are abducted ($\Delta x_\mathrm{R}, \Delta x_\mathrm{L} > 0$), the right VF is adducted and the left one is medialized ($\Delta x_\mathrm{R} > 0$ and $\Delta x_\mathrm{L} = 0$) and vice versa, and both VFs are tightly adducted ($\Delta x_\mathrm{R}, \Delta x_\mathrm{L} = 0$).

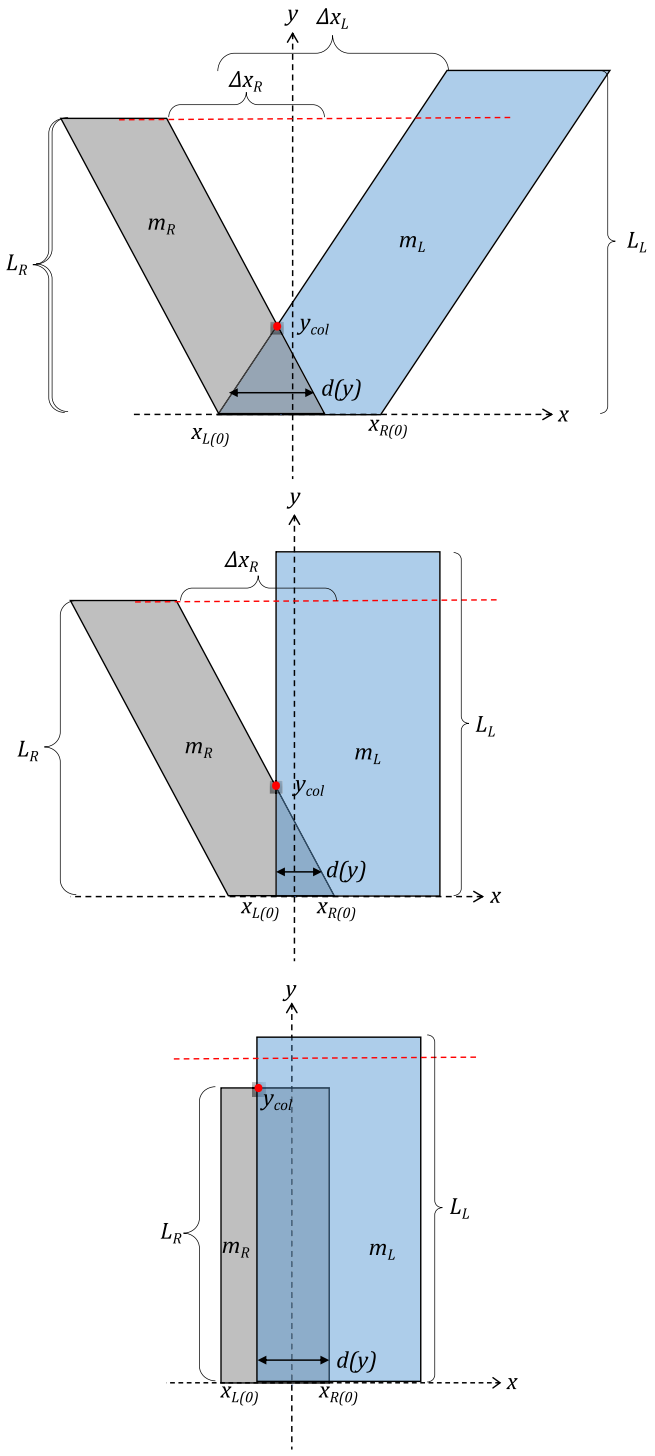

FIG. 11. (Color online) The three collision scenarios in the a-TBCM determined by the left/right posterior displacements: (Top) case $\Delta x_\mathrm{R}, \Delta x_\mathrm{L} > 0$, (middle) $\Delta x_\mathrm{R} > 0$ and $\Delta x_\mathrm{L} = 0$ (and vice versa), and (bottom) $\Delta x_\mathrm{R}, \Delta x_\mathrm{L} = 0$.

For the cases where at least one of the VFs has an adduction degree: ($\Delta x_i \neq 0$), the collision height is calculated from the interpenetration distance condition

https://doi.org/10.1121/10.0028164

$$d_R(y_{col}) = 0, \tag{A17}$$

with some algebra:

$$y_{col} = \frac{c_L - c_R}{b_R - b_L} = -\frac{c^*}{b^*}. \tag{A18}$$

For the case of parallel VFs, i.e., the case for $\Delta x_L = \Delta x_R = 0$. The collision height is calculated simply based on the collision condition and the length of the VF:

$$y_{col} = \begin{cases} \min(L_L, L_R) & \text{if} \quad d_R(0) \geq 0, \\ 0 & \text{if} \quad d_R(0) < 0. \end{cases} \tag{A19}$$

The effective spring collision constant in Eq. (A11) is computed assuming an in-series spring configuration

$$\frac{1}{k^*_{col}} = \frac{1}{k_{col_L}} + \frac{1}{k_{col_R}}, \tag{A20}$$

which comprises the contributions from the left- and right-side collision springs. The values for k_{col_R}, k_{col_L}, and η_{col} are computed following Galindo *et al.* (2017).

Replacing the Eqs. (A15) and (A20) in the integral in Eq. (A11) the total collision force can be computed by

$$F_{col} = -k^*_{col} y_{col} \left(c^* + \frac{b^* y_{col}}{2} \right) \times \left[1 + \eta_{col} \left(2c^{*2} + 2b^* c^* y_{col} + \frac{b^{*2} y^2_{col}}{2} \right) \right]. \tag{A21}$$

Note that the quantities c^*, b^*, k^*_{col}, and y_{col} have information on the properties of both VFs.

APPENDIX B: LIST OF ACRONYMS, SYMBOLS, AND SUBSCRIPTS

Tables II and III present the list of acronyms, symbols, and subscripts used in this work.

TABLE II. List of acronyms and their meanings.

Acronyms	Meaning	Acronyms	Meaning
VF	Vocal fold	*AA*	Amplitude asymmetry
TBCM	Triangular body cover model	*PA*	Phase asymmetry
a-TBCM	Asymmetric TBCM	*OQ*	Open quotient
CT	Cricothyroid	f_o	Fundamental frequency
TA	Thyroarytenoid	HSV	High-speed video
LCA	Lateral cricoarytenoid	DKG	Digital kymogram
IA	Interarytenoid	*PGO*	Posterior glottal opening
PCA	Posterior cricoarytenoid	*MGO*	Membranous glottal opening

TABLE III. List of symbols and subscripts, and their meanings.

Symbols	Meaning	Subscripts	Meaning
q	Asymmetry factor	R	Right side
m	Mass	L	Left side
k	Spring	$p2$, 02	Posterior wall, vocal process
d	Damping	u	Upper block
F	Force	l	Lower block
x	Position in x axis	b	Body block
y	Position in y axis	c	Coupling component
Δx	Posterior displacement	col	Collision component
$\vec{a}$	Muscle activation vector	k	Elastic component
L	Vocal fold length	d	Damping component
T	Vocal fold thickness	e	Aerodynamic component
α	Collision portion	t	Transversal component
A	Area	g	Glottal component

Alzamendi, G. A., Peterson, S. D., Erath, B. D., Hillman, R. E., and Zañartu, M. (**2022**). "Triangular body-cover model of the vocal folds with coordinated activation of the five intrinsic laryngeal muscles," J. Acoust. Soc. Am. **151**(1), 17–30.

Birkholz, P. (**2016**). "Glottalimageexplorer an open source tool for glottis segmentation in endoscopic high-speed videos of the vocal folds," in *Studientexte Zur Sprachkommunikation: Elektronische Sprachsignalverarbeitung 2016*, edited by O. Jokisch (TUDpress, Dresden), pp. 39–44.

Birkholz, P., Kröger, B. J., and Neuschaefer-Rube, C. (**2011**). "Synthesis of breathy, normal, and pressed phonation using a two-mass model with a triangular glottis," in *Interspeech 2011: 12th Annual Conference of the International Speech Communication Association*, Florence, Italy, pp. 2681–2684.

Bonilha, H. S., Deliyski, D. D., and Gerlach, T. T. (**2008**). "Phase asymmetries in normophonic speakers: Visual judgments and objective findings," Am. J. Speech. Lang. Pathol. **17**(4), 367–376.

Bonilha, H. S., Deliyski, D. D., Whiteside, J. P., and Gerlach, T. T. (**2012**). "Vocal fold phase asymmetries in patients with voice disorders: A study across visualization techniques," Am. J. Speech. Lang. Pathol. **21**(1), 3–15.

Calvache, C., Solaque, L., Velasco, A., and Peñuela, L. (**2023**). "Biomechanical models to represent vocal physiology: A systematic review," J. Voice **37**, 465.e1–465.e18.

Chen, Y., Li, Z., Chang, S., Rousseau, B., and Luo, H. (**2020**). "A reduced-order flow model for vocal fold vibration: From idealized to subject-specific models," J. Fluids Struct. **94**, 102940.

Chhetri, D. K., Berke, G. S., Lotfizadeh, A., and Goodyer, E. (**2009**). "Control of vocal fold cover stiffness by laryngeal muscles: A preliminary study," Laryngoscope **119**(1), 222–227.

Chhetri, D. K., Neubauer, J., and Sofer, E. (**2014a**). "Influence of asymmetric recurrent laryngeal nerve stimulation on vibration, acoustics, and aerodynamics," Laryngoscope **124**(11), 2544–2550.

Chhetri, D. K., Neubauer, J., Sofer, E., and Berry, D. A. (**2014b**). "Influence and interactions of laryngeal adductors and cricothyroid muscles on fundamental frequency and glottal posture control," J. Acoust. Soc. Am. **135**(4), 2052–2064.

Chhetri, D. K., and Park, S. J. (**2016**). "Interactions of subglottal pressure and neuromuscular activation on fundamental frequency and intensity," Laryngoscope **126**(5), 1123–1130.

Chung, H. R., Lee, Y., Reddy, N. K., Zhang, Z., and Chhetri, D. K. (**2024**). "Effects of thyroarytenoid activation induced vibratory asymmetry on voice acoustics and perception," Laryngoscope **134**(3), 1327–1332.

Desjardins, M., Apfelbach, C., Rubino, M., and Abbott, K. V. (**2022**). "Integrative review and framework of suggested mechanisms in primary muscle tension dysphonia," J. Speech. Lang. Hear. Res. **65**(5), 1867–1893.

Döllinger, M., Berry, D. A., and Kniesburges, S. (**2016**). "Dynamic vocal fold parameters with changing adduction in *ex-vivo* hemilarynx experiments," J. Acoust. Soc. Am. **139**(5), 2372–2385.

Döllinger, M., Zhang, Z., Schoder, S., Šidlof, P., Tur, B., and Kniesburges, S. (**2023**). "Overview on state-of-the-art numerical modeling of the phonation process," Acta Acust. **7**, 25.
Dresel, C., Mergell, P., Hoppe, U., and Eysholdt, U. (**2006**). "An asymmetric smooth contour two-mass model for recurrent laryngeal nerve paralysis," Logopedics Phoniatrics Vocology **31**(2), 61–75.
Erath, B., Zañartu, M., Peterson, S., and Plesniak, M. (**2011**). "Nonlinear vocal fold dynamics resulting from asymmetric fluid loading on a two-mass model of speech," Chaos **21**, 033113.
Erath, B. D., Peterson, S. D., Weiland, K. S., Plesniak, M. W., and Zañartu, M. (**2019**). "An acoustic source model for asymmetric intraglottal flow with application to reduced-order models of the vocal folds," PLoS One **14**(7), e0219914–e0219927.
Erath, B. D., Zañartu, M., Stewart, K. C., Plesniak, M. W., Sommer, D. E., and Peterson, S. D. (**2013**). "A review of lumped-element models of voiced speech," Speech Commun. **55**(5), 667–690.
Galindo, G. E., Peterson, S. D., Erath, B. D., Castro, C., Hillman, R. E., and Zañartu, M. (**2017**). "Modeling the pathophysiology of phonotraumatic vocal hyperfunction with a triangular glottal model of the vocal folds," J. Speech. Lang. Hear. Res. **60**(9), 2452–2471.
Geng, B., Pham, N., Xue, Q., and Zheng, X. (**2020**). "A three-dimensional vocal fold posturing model based on muscle mechanics and magnetic resonance imaging of a canine larynx," J. Acoust. Soc. Am. **147**(4), 2597–2608.
Hillel, A. D. (**2001**). "The study of laryngeal muscle activity in normal human subjects and in patients with laryngeal dystonia using multiple fine-wire electromyography," Laryngoscope **111**(S97), 1–47.
Horáček, J., Laukkanen, A. M., and Šidlof, P. (**2007**). "Estimation of impact stress using an aeroelastic model of voice production," Logopedics Phoniatrics Vocology **32**(4), 185–192.
Hsiung, M.-W., and Hsiao, Y.-C. (**2004**). "The characteristic features of muscle tension dysphonia before and after surgery in benign lesions of the vocal fold," ORL **66**(5), 246–254.
Hunter, E. J., Titze, I. R., and Alipour, F. (**2004**). "A three-dimensional model of vocal fold abduction/adduction," J. Acoust. Soc. Am. **115**(4), 1747–1759.
Ivey, C. M. (**2019**). "Vocal fold paresis," Otolaryngol. Clin. North Am. **52**(4), 637–648.
Ji, M., Liu, B., Jiang, J., Hoffman, M. R., Lan, J., and Fang, J. (**2022**). "Effect of controlled muscle activation in a unilateral vocal fold polyp setting on vocal fold vibration," Appl. Sci. **12**(23), 12486.
Jiang, J. J., Zhang, Y., and McGilligan, C. (**2006**). "Chaos in voice, from modeling to measurement," J. Voice **20**(1), 2–17.
Li, S., Scherer, R. C., Wan, M., Wang, S., and Song, B. (**2020**). "Intraglottal pressure: A comparison between male and female larynxes," J. Voice **34**(6), 813–822.
Lohscheller, J., Eysholdt, U., Toy, H., and Dollinger, M. (**2008**). "Phonovibrography: Mapping high-speed movies of vocal fold vibrations into 2-D diagrams for visualizing and analyzing the underlying laryngeal dynamics," IEEE Trans. Med. Imaging **27**(3), 300–309.
Lucero, J. C., Pelorson, X., and Van Hirtum, A. (**2020**). "Phonation threshold pressure at large asymmetries of the vocal folds," Biomed. Signal Process. Control **62**, 102105.
Lucero, J. C., and Schoentgen, J. (**2015**). "Smoothness of an equation for the glottal flow rate versus the glottal area," J. Acoust. Soc. Am. **137**(5), 2970–2973.
Malinowski, J., Pietruszewska, W., Kowalczyk, M., and Niebudek-Bogusz, E. (**2024**). "Value of high-speed videoendoscopy as an auxiliary tool in differentiation of benign and malignant unilateral vocal lesions," J. Cancer Res. Clin. Oncol. **150**(1), 10.
Manríquez, R., Peterson, S. D., Prado, P., Orio, P., Galindo, G. E., and Zañartu, M. (**2019**). "Neurophysiological muscle activation scheme for controlling vocal fold models," IEEE Trans. Neural Syst. Rehabil. Eng. **27**(5), 1043–1052.
McCollum, I., Throop, A., Badr, D., and Zakerzadeh, R. (**2023**). "Gender in human phonation: Fluid–structure interaction and vocal fold morphology," Phys. Fluids **35**(4), 041907.
Mehta, D. D., Zañartu, M., Quatieri, T. F., Deliyski, D. D., and Hillman, R. E. (**2011**). "Investigating acoustic correlates of human vocal fold vibratory phase asymmetry through modeling and laryngeal high-speed videoendoscopy," J. Acoust. Soc. Am. **130**(6), 3999–4009.
Movahhedi, M., Geng, B., Xue, Q., and Zheng, X. (**2021**). "Effects of cricothyroid and thyroarytenoid interaction on voice control: Muscle activity, vocal fold biomechanics, flow, and acoustics," J. Acoust. Soc. Am. **150**(1), 29–42.
Palaparthi, A., Smith, S., Mau, T., and Titze, I. R. (**2019**). "A computational study of depth of vibration into vocal fold tissues," J. Acoust. Soc. Am. **145**(2), 881–891.
Perrine, B. L., and Scherer, R. C. (**2023**). "Using a vertical three-mass computational model of the vocal folds to match human phonation of three adult males," J. Acoust. Soc. Am. **154**(3), 1505–1525.
Pickup, B. A., and Thomson, S. L. (**2009**). "Influence of asymmetric stiffness on the structural and aerodynamic response of synthetic vocal fold models," J. Biomech. **42**(14), 2219–2225.
Poletto, C. J., Verdun, L. P., Strominger, R., and Ludlow, C. L. (**2004**). "Correspondence between laryngeal vocal fold movement and muscle activity during speech and nonspeech gestures," J. Appl. Physiol. **97**(3), 858–866.
Qiu, Q., Schutte, H., Gu, L., and Yu, Q. (**2003**). "An automatic method to quantify the vibration properties of human vocal folds via videokymography," Folia Phoniatr. Logop. **55**(3), 128–136.
Samlan, R. A., and Story, B. H. (**2017**). "Influence of left-right asymmetries on voice quality in simulated paramedian vocal fold paralysis," J. Speech. Lang. Hear. Res. **60**(2), 306–321.
Samlan, R. A., Story, B. H., Lotto, A. J., and Bunton, K. (**2014**). "Acoustic and perceptual effects of left–right laryngeal asymmetries based on computational modeling," J. Speech. Lang. Hear. Res. **57**(5), 1619–1637.
Schlegel, P., Berry, D. A., and Chhetri, D. K. (**2022**). "Analysis of vibratory mode changes in symmetric and asymmetric activation of the canine larynx," PLoS One **17**(4), e0266910.
Sommer, D. E., Erath, B. D., Zañartu, M., and Peterson, S. D. (**2013**). "The impact of glottal area discontinuities on block-type vocal fold models with asymmetric tissue properties," J. Acoust. Soc. Am. **133**(3), EL214–EL220.
Spencer, M. L. (**2015**). "Muscle tension dysphonia: A rationale for symptomatic subtypes, expedited treatment, and increased therapy compliance," Perspect. Voice Voice Dis. **25**(1), 5–15.
Steinecke, I., and Herzel, H. (**1995**). "Bifurcations in an asymmetric vocal-fold model," J. Acoust. Soc. Am. **97**(3), 1874–1884.
Story, B. H. (**2002**). "An overview of the physiology, physics and modeling of the sound source for vowels," Acoust. Sci. Tech. **23**(4), 195–206.
Story, B. H. (**2008**). "Comparison of magnetic resonance imaging-based vocal tract area functions obtained from the same speaker in 1994 and 2002," J. Acoust. Soc. Am. **123**(1), 327–335.
Story, B. H. (**2015**). "Mechanisms of voice production," in *The Handbook of Speech Production* (Wiley, New York), pp. 34–58.
Story, B. H., and Titze, I. R. (**1995**). "Voice simulation with a body-cover model of the vocal folds," J. Acoust. Soc. Am. **97**(2), 1249–1260.
Story, B. H., Titze, I. R., and Hoffman, E. A. (**1998**). "Vocal tract area functions for an adult female speaker based on volumetric imaging," J. Acoust. Soc. Am. **104**(1), 471–487.
Tao, C., and Jiang, J. J. (**2007**). "Mechanical stress during phonation in a self-oscillating finite-element vocal fold model," J. Biomech. **40**(10), 2191–2198.
Tipton, P. W., Ekbom, D. C., Rutt, A. L., and van Gerpen, J. A. (**2020**). "Vocal fold 'paralysis': An early sign in multiple system atrophy," J. Voice **34**(6), 940–944
Titze, I. R. (**2002**). "Regulating glottal airflow in phonation: Application of the maximum power transfer theorem to a low dimensional phonation model," J. Acoust. Soc. Am. **111**(1), 367–376.
Titze, I. R., and Hunter, E. J. (**2007**). "A two-dimensional biomechanical model of vocal fold posturing," J. Acoust. Soc. Am. **121**(4), 2254–2260.
Titze, I. R., and Story, B. H. (**2002**). "Rules for controlling low-dimensional vocal fold models with muscle activation," J. Acoust. Soc. Am. **112**(3), 1064–1076.
Vampola, T., Horáček, J., and Klepáček, I. (**2016**). "Computer simulation of mucosal waves on vibrating human vocal folds," Biocybern. Biomed. Eng. **36**(3), 451–465.
Wade, L., Hanna, N., Smith, J., and Wolfe, J. (**2017**). "The role of vocal tract and subglottal resonances in producing vocal instabilities," J. Acoust. Soc. Am. **141**(3), 1546–1559.
Xue, Q., Mittal, R., Zheng, X., and Bielamowicz, S. (**2010**). "A computational study of the effect of vocal-fold asymmetry on phonation," J. Acoust. Soc. Am. **128**(2), 818–827.

Yokota, K., Ishikawa, S., Koba, Y., Kijimoto, S., and Sugiki, S. (**2019**). "Inverse analysis of vocal sound source using an analytical model of the vocal tract," Appl. Acoust. **150**, 89–103.
Zañartu, M., Galindo, G. E., Erath, B. D., Peterson, S. D., Wodicka, G. R., and Hillman, R. E. (**2014**). "Modeling the effects of a posterior glottal opening on vocal fold dynamics with implications for vocal hyperfunction," J. Acoust. Soc. Am. **136**(6), 3262–3271.
Zañartu, M., Mehta, D. D., Ho, J. C., Wodicka, G. R., and Hillman, R. E. (**2011**). "Observation and analysis of *in vivo* vocal fold tissue instabilities produced by nonlinear source-filter coupling: A case study," J. Acoust. Soc. Am. **129**(1), 326–339.
Zañartu, M., Mongeau, L., and Wodicka, G. R. (**2007**). "Influence of acoustic loading on an effective single mass model of the vocal folds," J. Acoust. Soc. Am. **121**(2), 1119–1129.
Zhang, Y., and Jiang, J. J. (**2004**). "Chaotic vibrations of a vocal fold model with a unilateral polyp," J. Acoust. Soc. Am. **115**(3), 1266–1269.
Zhang, Z. (**2016a**). "Cause-effect relationship between vocal fold physiology and voice production in a three-dimensional phonation model," J. Acoust. Soc. Am. **139**(4), 1493–1507.
Zhang, Z. (**2016b**). "Mechanics of human voice production and control," J. Acoust. Soc. Am. **140**, 2614–2635.
Zhang, Z. (**2018**). "Vocal instabilities in a three-dimensional body-cover phonation model," J. Acoust. Soc. Am. **144**(3), 1216–1230.
Zhang, Z. (**2021**). "Contribution of laryngeal size to differences between male and female voice production," J. Acoust. Soc. Am. **150**(6), 4511–4521.
Zhang, Z. (**2023**). "Vocal fold vertical thickness in human voice production and control: A review," J. Voice. (published online).
Zhang, Z., and Luu, T. H. (**2012**). "Asymmetric vibration in a two-layer vocal fold model with left-right stiffness asymmetry: Experiment and simulation," J. Acoust. Soc. Am. **132**(3), 1626–1635.